Available online at www.sciencedirect.com
ScienceDirect
Journal of Photochemistry and Photobiology A: Chemistry 183 (2006) 225–235
Journal of Photochemistry and Photobiology A:Chemistry
www.elsevier.com/locate/jphotochem

Photophysical properties of 2,6-dicyano-*N*,*N*,*N*′,*N*′-tetramethyl-*p*-phenylenediamine

A. Rosspeintner, G. Angulo[1], M. Weiglhofer, S. Landgraf, G. Grampp*

Institute of Physical and Theoretical Chemistry, TU-Graz, Technikerstrasse 4, 8010 Graz, Austria

Received 30 September 2005; received in revised form 14 March 2006; accepted 15 March 2006
Available online 29 March 2006

Abstract

Photophysical properties of 2,6-dicyano-*N*,*N*,*N*′,*N*′-tetramethyl-*p*-phenylenediamine (DCTMPPD) are reported. Fluorescence quantum yields range from 0.37 to 0.58 and fluorescence lifetimes from 12.2 to 22.9 ns in 28 different solvents. The triplet energy is determined to be 16.8 kK. Steady-state and time-resolved emission anisotropies in glycerol are given. Three correlation times with $\tau_1 < 0.8$ ns $\tau_2 = 20$ ns and $\tau_3 > 80$ ns are found. The fluorescence solvatochromism is analyzed using empirical one- and multiparameter approaches as well as classical non-empirical continuum models. The excited state dipole moment is estimated to be between 10 and 12 D, depending on the model applied. The ground state pK_a is determined to be 2.5, while for the excited state pK_a^* a range of 0.5–2 can be estimated.

Keywords: 2,6-Dicyano-*N*,*N*,*N*′,*N*′-tetramethyl-*p*-phenylenediamine; Anisotropy; Solvatochromism; Photophysical properties

1. Introduction

For many reasons *p*-phenlyenediamines are an important class of compounds. They establish well-defined reversible two-step redox systems, as already pointed out by Michaelis et al. [1,2] in a series of significant papers in the mid-30s. Under oxidation the diamines (*R*) form stable colored semiquinone radical cations ($S^{+\bullet}$, Wurster's salts) and the additional withdraw of an electron results in the colorless quinonediamines (T). These redox properties and their low oxidation potentials make *p*-phenlyenediamines suitable as developers of color films and slides, for example. Redox potentials vary according to the various substituents [3,4] and especially the *N*,*N*,*N*′,*N*′-tetramethyl-*p*-phenylenediamine (TMPPD) is widely used as an excellent electron donor, both in forming charge transfer complexes and in photoinduced electron transfer reactions.

Many physical properties of these compounds, as e.g. redox potentials, p*K*-values, extinction coefficients, of both *R* and $S^{+\bullet}$, etc. are reported in the literature [3,5]. ESR-coupling constants and the corresponding spin densities have been measured and interpreted in great detail [6]. Photoionization, CIDEP (chemically induced dynamic electron polarization) and MARY (magnetic field dependent reaction yield)[7] studies are reported on these substances, mainly on TMPPD [8–10], but to the best of our knowledge, no highly fluorescing *p*-phenlyenediamine derivative has been observed and studied up to now. In this paper we report the basic photophysical aspects of the first highly fluorescent *p*-phenlyenediamine derivative, the 2,6-dicyano-*N*,*N*,*N*′,*N*′-tetramethyl-*p*-phenylenediamine (DCTMPPD).

From another point of view, DCTMPPD can be considered as pertaining to the family of amino substituted cyano-benzenes, which are of enormous photochemical interest. *p*-Cyano-*N*,*N*-dimethylaniline (DMABN) is one of the most studied fluorescing molecules [11] due to its fascinating dual fluorescence properties. Unlike DMABN, DCTMPPD does not demonstrate this feature in the polarity range studied.

From the comparison between benzene, anilines (including phenylenediamines), and cyano-anilines it becomes obvious that the combination of the electron withdrawing cyano group and the electron donating amino group, or its methylated form, dramatically increase both fluorescence quantum yield and lifetime. In fact, the excited state dipole moments are usually notably larger than the ground state ones. One of the

* Corresponding author. Tel.: +43 316 873 8222; fax: +43 316 873 8225.
E-mail address: grampp@ptc.tugraz.at (G. Grampp).
[1] Present address: Facultad de Ciencias del Medio Ambiente, Universidad de Castilla-La Mancha, Spain.

1010-6030/$ – see front matter © 2006 Elsevier B.V. All rights reserved.
doi:10.1016/j.jphotochem.2006.03.020

aims of this paper is to find the excited state dipole moment of DCTMPPD from classical Stokes shift analysis in several solvents.

This article is meant to be a collection of most of the properties of interest in photochemical and photokinetic studies in solution related to DCTMPPD.

2. Experimental

2, 6- Dicyano- N, N, N', N' -tetramethyl-*p*-phenylenediamine was synthesized and purified as described elsewhere [12]. Solvents were freshly distilled and dried over molecular sieve. $HClO_4$ (Merck, 70%), citric acid monohydrate ($\geq$ 99.5% p.a., Roth) and Na_2HPO_4 ($\geq$ 99.0% purum p.a., Fluka) were used as received. pH values of aeqeous solutions were either measured using a pH-electrode (pH > 3) or determined via titration with 0.4 M NaOH Merck standard.

All solutions were deaerated with Ar for 15 min immediately before each measurement to avoid quenching caused by oxygen. The measurements were carried out in septa-sealed quartz cuvettes (10 mm Suprasil glass). The concentration of DCTMPPD was always chosen such that the absorption at the excitation wavelength did not exceed 0.10, corresponding to a maximum concentration of 3×10^{-5} M. All experiments were performed at 25 °C except for the measurements in glycerol (anisotropy, Time resolved area normalized emission spectra (TRANES)), which were conducted at 20 °C.

Absorption spectra were recorded with a Shimadzu UV-3101PC UV-VIS-NIR spectrophotometer (bandpass 1 nm). Corrected fluorescence and excitation spectra were recorded with a Jobin–Yvon Spex FluoroMax-2 spectrofluorimeter (scan range from 250 to 900 nm, bandpass 2 nm). The solid state luminescence measurements (77 K) were obtained on a multifunctional spectrofluorometric system [13]. Gas phase measurements were performed in a home-built apparatus similar to the one described in Ref. [14], which was attached to the FluoroMax-2 spectrofluorimeter.

Lifetime measurements were performed on a home-built modulation spectrofluorometer and a single photon counting apparatus, both described elsewhere [15]. For time resolved anisotropy and time-resolved emission spectra (TRANES) a PicoQuant 397 nm pulsed Laser diode was used as vertically polarized excitation light source. A total of 15 million counts (in 4096 channels) were recorded in every individual experiment to secure a good signal to noise ratio, even at long times; thus, about 60,000 counts are recorded in the channel of maximum intensity. TRANES were recorded with the emission polarizer set at the magic angle condition (54.7°). For the proper choice of the emission wavelength six different interference filters (10 nm FWHM) were used. The validity of the polarizer settings in steady-state and time-resolved anisotropy experiments was checked using a diluted scattering sample. The corresponding anisotropies were found to be well above 0.97 [16].

Fluorescence quantum yields were determined using a deaerated solution of Coumarin 6 in ethanol as a reference standard ($\Phi_R = 0.78$ [17]). The following equation [18,19], the validity of which was recently approved by Kotelevskiy [20], was applied:

$$\Phi_s = \frac{I_s}{I_r}\frac{(1-10^{-OD_r})}{(1-10^{-OD_s})}\left(\frac{n_s}{n_r}\right)^2 \Phi_r \quad (1)$$

where I is the emission intensity, was calculated from the integrated corrected spectrum area, OD represents the optical density at the excitation wavelength and n_X the refractive index at 25 °C of the corresponding solvent. The subscripts s and r refer to the sample and to the reference, respectively. The optical density at and beyond the excitation wavelength did not exceed 0.10.

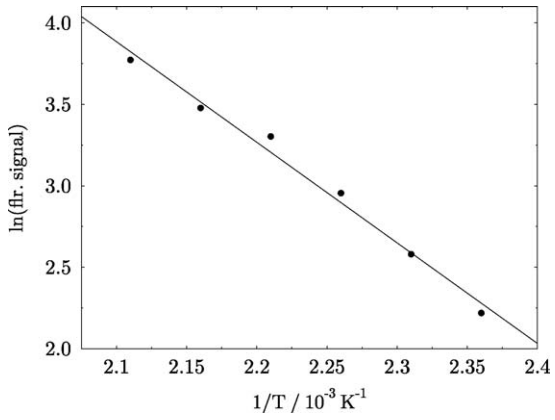

Fig. 1. Clausius–Clapeyron representation of gas-phase fluorescence intensities of DCTMPPD at different temperatures.

3. Results and discussion

3.1. Sublimation enthalpy

The dependence of gas-phase fluorescence intensity, I_{fl}, on temperature was monitored and found to agree with the Clausius–Clapeyron relation [14,21]

$$\frac{d\ln p}{dT} = \frac{d\ln(I_{fl})}{dT} = \frac{\Delta_{vap}H}{RT^2}, \quad (2)$$

where $\Delta_{vap}H$ is the sublimation enthalpy and p, R and T are pressure, gas constant and thermodynamic temperature. As it was impossible to monitor the pressure directly, it was assumed that at the lowest pressures achieved (300 Pa) the fluorescence intensity and the pressure were directly proportional. To check the validity of this method the sublimation enthalpy of anthracene was determined and compared to recent literature results [22]. The obtained 84 kJ/mol were within the range of sublimation enthalpies obtained by common methods. The sublimation enthalpy of DCTMPPD amounts to 52 kJ/mol (see Fig. 1).

3.2. Fluorescence anisotropy

Fluorescence depolarization following excitation with polarized light gives useful information on (i) the relative position of absorption and emission transition dipole moments, which is obtainable from the maximum anisotropy, r_0, (ii) the molecular size and (iii) the nature of the electronic transitions from the

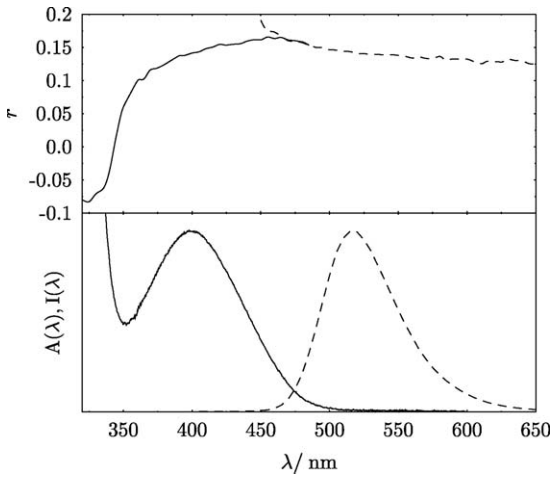

Fig. 2. Excitation (—) and emission (- - -) anisotropy in glycerol at 20 °C, with $\lambda_{em} = 520$ nm and $\lambda_{exc} = 400$ nm, respectively. The shape of r is independent of both emission and excitation wavelength. Absorption, ($A(\lambda)$, —), and fluorescence, ($I(\lambda)$, - - -), spectra of DCTMPPD in glycerol are given for the sake of clarity in the lower graph.

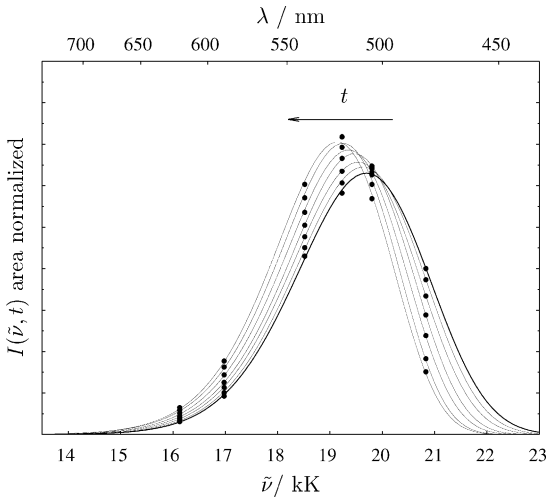

Fig. 3. Time resolved area normalized emission spectra (TRANES) of DCTMPPD in glycerol. (●) Denote the experimental points, while (—) denote the corresponding fits using the log-normal function. The times represented are 0, 0.1, 0.3, 0.5, 1, 2 and 10 ns in order of decreasing peak energy.

exitation polarization spectrum. Especially the latter property is essential for subsequent solvent shift analyses.

3.2.1. Steady-state anisotropy

The anisotropy, in the most general case, is given by:

$$r = \frac{I_{VV} - G I_{VH}}{I_{VV} + 2G I_{VH}}, \tag{3}$$

where $G = I_{HV}/I_{HH}$ and for example I_{HV} corresponds to horizontally polarized excitation and vertically polarized emission. The steady state excitation anisotropy spectrum of DCTMPPD in glycerol is given in Fig. 2 and shows only a slight change of anisotropy across the lowest energy absorption transition. Obviously the latter pertains only to one transition ($S_0 \rightarrow S_1$). The absolute value of the resulting steady-state anisotropy is much lower than r_0 due to rotational and librational depolarization, which are still active even in highly viscous glycerol solutions, as will be seen from the time resolved measurements.

The steady-state emission anisotropy, also shown in Fig. 2 for completeness, indicates that, as in the aforementioned absorption, a simple two-state transition ($S_0 \leftarrow S_1$) is observed. The increasing anisotropy at the blue edge of the emission is due to solvent relaxation causing a dynamic Stokes-shift [16]. To confirm this statement time-resolved area normalized emission spectra (TRANES), shown in Fig. 3, were conducted. The TRANES were obtained by fitting the corresponding fluorescence decays following the usual procedure for time resolved emission spectra (TRES) as described e.g. in [16] and adding as final step the normalization to the area of the corresponding TRES [23,24]. For a better guidance of the reader's eye the experimental data points were then fitted using the log-normal function [25]. No isoemissive points can be observed indicating that a continuum of species, as usual for solvent relaxation in viscous media, is involved in the relaxation process [26].

3.2.2. Time-resolved emission anisotropy

For the time resolved measurements a simplified version of Eq. (3) was used ($G = 1$). The modular set-up[15] allows a fixed position of the emission polarizer and the detection system. Whenever the polarizer is changed from the vertical to the horizontal position, the detection system thus is changed too, thereby avoiding a manifestation of the photomultiplier sensitivity-dependence on differently polarized light. From the various methods of time resolved anisotropy decay parameter extraction the direct $r(t)$-decay analysis was chosen. All other analysis methods as e.g. direct analysis of $I_{\parallel}$ and $I_{\perp}$, or analysis of $I_{\parallel} - I_{\perp}$ and $I_{\parallel} + 2I_{\perp}$ were rejected due to the complicated overlap of time-dependent spectral relaxation (cf. Fig. 3) and anisotropy decay resulting in the necessity to use up to five exponentials for fitting.

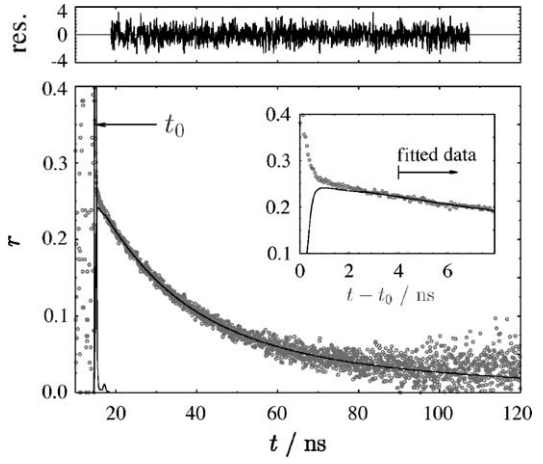

Fig. 4. Time resolved anisotropy of DCTMPPD in glycerol at 20 °C, including the long time fit to $r(t)$, using Eq. (5), and the instrument response function. The emission was observed through a 520 nm interference filter (ca. 10 nm bandpass). Weighted residuals are given for the fitting range. The inlet shows the short time behaviour.

Fig. 4 shows the anisotropy decay, $r(t)$ including the weighted residuals, accounting for the propagation of the individual measurements' Poisson errors. The corresponding weighting factor for channel i, $w(i)$, is given by [27]:

$$w(i) = \frac{3(I_{\parallel}(i) + 2I_{\perp}(i))}{(2 + 3r(i) - 3r(i)^2 - 2r(i)^3)} \tag{4}$$

A direct analysis of the anisotropy decay is not suitable for extracting correlation times close to the width of the instrument response function [16,28]. Therefore the fitting range was limited to the long time regime ($t > 4$ ns). This limitation allows the determination of one and a crude estimation of a second correlation time, τ_i^{rot}, and permits an estimation of r_0. The third observable but not analyzable fast correlation time, too fast (< 800 ps) to be associated with rotational diffusion of DCTMPPD, is probably a manifestation of very fast librational motions of the fluorophore within the solvent cage. In the following it is supposed (i) that DCTMPPD is sufficiently well described by an ellipsoid (semiaxes[2]: $a = 6.2$ Å, $b = 5.2$ Å, and $c = 3.8$ Å) whose two rotational diffusion coefficients about the two in-plane axes, $D_{\perp}$, (perpendicular to the symmetry axis) are similar and much smaller than the diffusion coefficient for rotation around the unique axis of symmetry, $D_{\parallel}$, (parallel to the symmetry axis), (ii) that the electronic transitions (absorption and emission) are polarized within the molecular plane with ϕ being the difference in their azimuthal angles and (iii) that the ultrafast depolarization component is excluded from the analysis. The resulting biexponential description of the anisotropy decay due to rotational diffusion is given by [29]:

$$r(t) = r(0)^{\mathrm{red}}(0.25\exp(-\underbrace{6D_{\perp}t}_{1/\tau_1^{\mathrm{rot}}}) + 0.75\cos 2\phi \times \exp(-\underbrace{(2D_{\perp} + 4D_{\parallel})t}_{1/\tau_2^{\mathrm{rot}}})), \tag{5}$$

where $r(0)^{\mathrm{red}}$ accounts for the reduced maximum anisotropy, which is due to the excluded ultrafast (non-rotationally diffusional) component. Applying this four-parameter model to the experimental anisotropy decay yields,

$$\tau_1^{\mathrm{rot}} = (6D_{\perp})^{-1} = 80 \pm 30\,\mathrm{ns} \quad D_{\perp} = (2.1 \pm 1.2) \times 10^6\,\mathrm{s}^{-1}$$
$$\tau_2^{\mathrm{rot}} = (2D_{\perp} + 4D_{\parallel})^{-1} = 20 \pm 1\,\mathrm{ns}$$
$$D_{\parallel} = (11.4 \pm 0.6) \times 10^6\,\mathrm{s}^{-1} \qquad r(0) = 0.25 \qquad \phi = 15^{\circ}$$

The limited time resolution of the apparatus allows only for an estimation of the absolute maximum anisotropy, $r(0)$. From Fig. 4 it is estimated to be larger than 0.35. Correspondingly the angle between the absorption and emission transition dipole moments, ϕ, is estimated to be smaller than 16°, which is in coherence with the above applied model.

[2] Semiaxes were determined by circumscribing the geometry optimized (MP2/6-311+G**) van der Waals surface of DCTMPPD with the ellipsoid of minimum superficies.

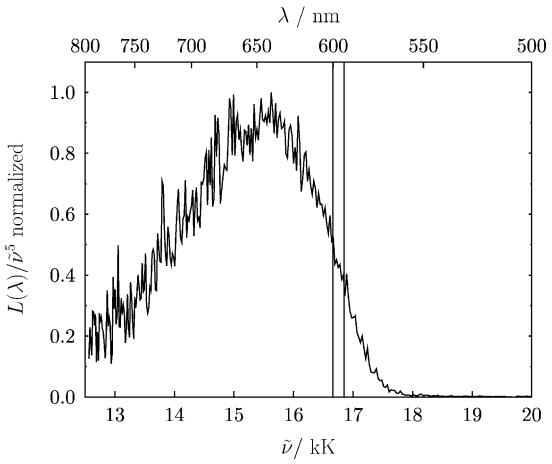

Fig. 5. Modified phosphorescence spectrum of DCTMPPD in *n*-propanol at 77 K. Vertical lines denote the errors for determination of the triplet energy, E_{T}.

3.3. Triplet energy, E_{T}

The triplet energy, E_{T}, was determined from the turning point of the solid state luminescence spectrum in *n*-propanol at 77 K to be 16.8 kK (cf. Fig. 5).

3.4. Condensed phase photophysical properties

The extinction coefficient, ϵ,[3] the fluorescence quantum yield, Φ_{F}, the fluorescence lifetime, τ_{F}, and the 0–0 energy, E_{00}, of DCTMPPD were determined in 28 different solvents, spanning a wide range of polarities (see Table 1). Additionally the centers of gravity of the fluorescence, $\tilde{\nu}_{\mathrm{f}}^{\mathrm{cg}}$, and the energetically lowest absorption band, $\tilde{\nu}_{\mathrm{a}}^{\mathrm{cg}}$, were determined by:

$$\tilde{\nu}_{\mathrm{f}}^{\mathrm{cg}} = \frac{\int I(\tilde{\nu})\tilde{\nu}\,\mathrm{d}\tilde{\nu}}{\int I(\tilde{\nu})\,\mathrm{d}\tilde{\nu}}, \qquad \tilde{\nu}_{\mathrm{a}}^{\mathrm{cg}} = \frac{\int \epsilon(\tilde{\nu})\tilde{\nu}\,\mathrm{d}\tilde{\nu}}{\int \epsilon(\tilde{\nu})\,\mathrm{d}\tilde{\nu}} \tag{6}$$

where $I(\tilde{\nu})$ and $\epsilon(\tilde{\nu})$ are the modified fluorescence and absorption spectra (see Fig. 6 for an example), respectively, given by [18,30]:

$$I(\tilde{\nu}) = \frac{I(\lambda)}{\tilde{\nu}^5}, \qquad \epsilon(\tilde{\nu}) = \frac{\epsilon(\lambda)}{\tilde{\nu}} \tag{7}$$

and used for further solvatochromic shift analyses. The energetically lowest lying absorption band was extracted by fitting with five Gaussians, four pertaining to the lowest energy transition band and the fifth accounting for the low energy shoulder of the adjacent absorption band. The 0–0 energy, E_{00}, was estimated taking the mean value of fluorescence and absorption centers of gravity,

$$E_{00} = \frac{\tilde{\nu}_{\mathrm{a}}^{\mathrm{cg}} + \tilde{\nu}_{\mathrm{f}}^{\mathrm{cg}}}{2}. \tag{8}$$

Additionally the radiative lifetimes, τ_{FM}, obtained by two different methods were compared. The first method to obtain the radiative, or intrinsic, fluorescence lifetime is simply being

[3] The extinction coefficient of DCTMPPD did not change with solvent and was evaluated to be $2700 \pm 300\,\mathrm{M}^{-1}\mathrm{cm}^{-1}$ using the Lambert–Beer law.

Table 1
The spectral and photophysical properties of DCTMPPD at 25 °C in solvents of different properties

No.	Solvent	α [31]	π^* [31]	$\tilde{\nu}_a^{cg}$ (kK)	$\tilde{\nu}_f^{cg}$ (kK)	E_{00} (kJ mol^{-1})	τ_F (ns)	Φ_F
1	Gas-phase (473 K)	0.00	−1.20	26.36	20.57	281	–	–
2	Acetone	0.08	0.62	25.65	19.05	267	21.3	0.51
3	Acetonitrile	0.19	0.66	25.58	18.87	266	21.8	0.53
4	Benzene	0.00	0.55	25.27	19.25	266	17.9	0.57
5	Benzonitrile	0.00	0.88	25.04	18.90	263	19.5	0.50
6	Butylacetate	0.00	0.46	25.65	19.35	269	18.7	0.52
7	Butylether	0.00	0.18	25.80	19.91	273	16.0	0.45
8	Cyclohexane	0.00	0.00	25.81	20.17	275	12.5	0.37
9	1,2-Dichloroethane	0.00	0.73	25.35	19.10	266	17.8	0.52
10	Dichloromethane	0.13	0.82	25.17	19.13	265	19.2	0.57
11	Diethylether	0.00	0.24	25.60	19.71	271	16.6	0.46
12	Dioxane	0.00	0.49	25.57	19.17	268	19.3	0.55
13	dmf[a]	0.00	0.88	25.41	18.73	264	21.8	0.57
14	dmso	0.00	1.00	25.20	18.58	262	22.9	0.55
15	Ethanol	0.86	0.54	25.53	18.93	266	21.3	0.51
16	Ethylacetate	0.00	0.45	25.66	19.26	269	19.1	0.49
17	Glycerin	1.21	0.62	24.79	18.27	258	20.4	0.54
18	Hexane	0.00	−0.11	25.86	20.25	276	12.7	0.38
19	*i*-Pentane	0.00	–	25.96	20.26	276	12.2	0.37
20	*i*-Propylether	0.00	0.19	25.86	19.88	274	14.8	0.39
21	Methanol	0.98	0.60	25.49	18.85	265	22.2	0.52
22	Octanol	0.77	0.40	25.42	19.11	266	19.1	0.58
23	pc	0.00	0.83	25.35	18.78	264	22.0	0.58
24	*n*-Pentylether	0.00	–	25.74	19.77	272	16.1	0.46
25	Propionitril	0.00	0.64	25.57	19.02	267	19.0	0.47
26	*n*-Propylether	0.00	0.27	25.65	19.70	271	16.0	0.55
27	thf	0.00	0.55	25.61	19.30	269	18.8	0.54
28	Toluene	0.00	0.49	25.30	19.35	267	17.5	0.55
29	H_2O (pH 7)	1.17	1.09	25.85	18.01	262	22.0	0.47
30	$H_2O/HClO_4$ (H_0 − 1)	–	–	26.40	20.00	277	4.0	0.06

[a] Used acrynoms: dmf: dimethylformamide; dmso: dimethylsulfoxide; pc: propylene carbonate; thf: tetrahydrofurane.

based on the definition of the fluorescence quantum yield, which is given by:

$$\Phi_F = \frac{\tau_F}{\tau_{FM}}, \tag{9}$$

where τ_{FM} and τ_F are the radiative and fluorescence lifetimes, respectively. The second approach is more theoretical, and estimates the radiative lifetime using the Strickler-Berg relation [32], which is given by

$$\frac{1}{\tau_{FM}} = \frac{8\pi 230cn^2}{N_L} \frac{\int I(\tilde{\nu})\,d\tilde{\nu}}{\int (I(\tilde{\nu})/\tilde{\nu}^3)\,d\tilde{\nu}} \int \frac{\epsilon(\tilde{\nu})}{\tilde{\nu}}\,d\tilde{\nu} \tag{10}$$

where $I(\tilde{\nu})$ and $\epsilon(\tilde{\nu})$ represent the fluorescence and absorption spectra, respectively. For the estimation of the radiative lifetime using Strickler's and Berg's equation the first absorption band, theoretically pertaining to the S_0–S_1 transition, is extracted as described above.

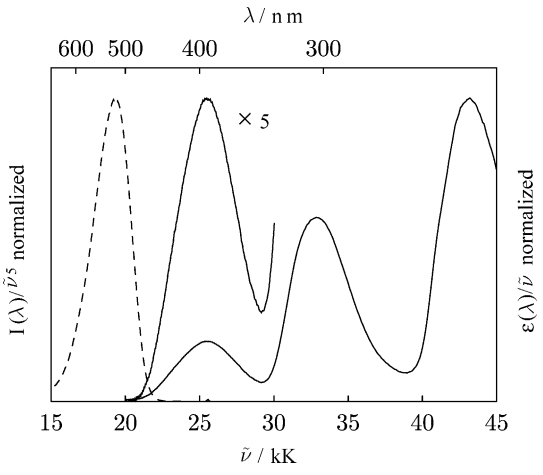

Fig. 6. Modified absorption (—) and fluorescence (- - -) spectra of DCTMPPD in acetonitrile.

Comparison of the experimentally, Eq. (9), and theoretically, Eq. (10), obtained values for the radiative lifetimes gives a reasonable linear relationship (not shown), thus justifying the usage of the Strickler-Berg relation and its inherent assumptions. The lowest energy absorption band shape changes from an almost gaussian shaped curve in polar solvents to a broad unstructured non-Gaussian curve in non-polar solvents (see Fig. 7). The interference of additional low lying excited states can be outruled due to the perfect congruence between absorption and excitation spectra and the flatness of the steady-state excitation anisotropy over the whole low energy absorption band, thus justifying the assumption of a two-level energy scheme.

3.5. Solvatochromism

The shift of spectra upon changing the solvent can be used to obtain important information on the solute's intrinsic photophys-

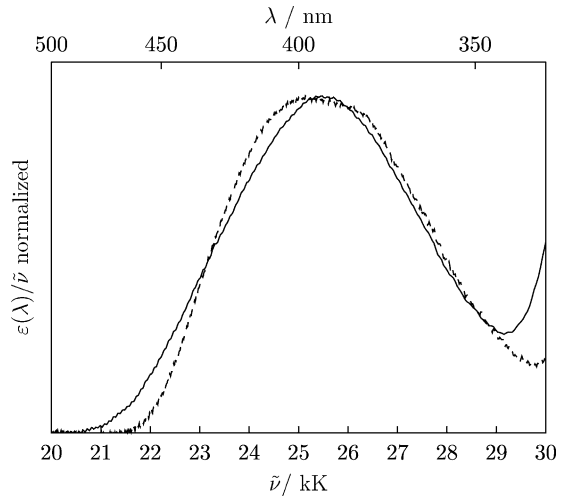

Fig. 7. Modified absorption spectra of DCTMPPD in acetonitrile (—) and cyclohexane (- - -).

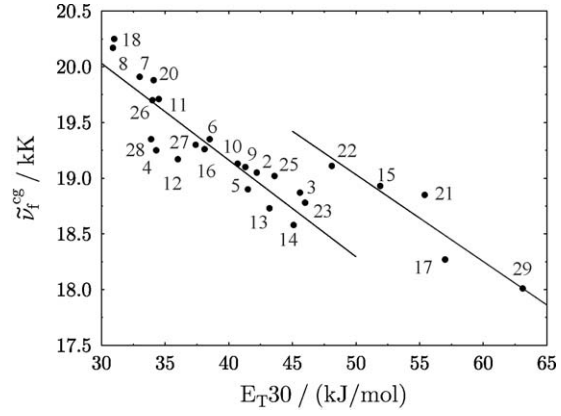

Fig. 8. E_T30 plot of all experimental fluorescence maxima. Note the shift of DCTMPPD in protic solvents (15, 17, 21, 22, 29).

ical characteristics and its specific and non-specific interactions with the solvent. Due to the above mentioned difficulties with absorption spectra only the fluorescence spectra were analyzed.

3.5.1. E_T30-scale

E_T30 plots are presented to get some insight into whether specific interactions (as e.g. H-bonding) have to be accounted for or not. Two distinct parallel lines are found in our E_T30 analysis (Fig. 8), one for non-protic solvents and one for protic solvents. This indicates merely that for the energetics of DCTMPPD specific solute–solvent interactions with protic solvents are less important than for the Reichardt betain dye [33].

3.5.2. Linear solvation energy relationship (LSER)

To get deeper qualitative and quantitative information on the type of solute–solvent interactions an analysis of the fluorescence centers of gravity using a multi-parameter approach introduced by Kamlet and Taft [34] was performed:

$$\tilde{\nu}_f^{cg} = \tilde{\nu}_f^{\circ} + s\pi^* + a\alpha + b\beta, \quad (11)$$

where $\tilde{\nu}_f^{cg}$ denotes the center of gravity of the corrected fluorescence spectrum, where π^* is a measure of the polarity/polarizability of the solvent. The α-scale is an index of solvent acidity (hydrogen bond donor ability) and the β-scale is an index of solvent basicity (hydrogen bond acceptor ability). While π^*, α and β denote the solvent properties for each of the above mentioned contributions for solute–solvent interactions, the coefficients s, a and b describe the corresponding solute's contributions. Therefore the advantage of the Kamlet–Taft treatment is obviously to sort out the quantitative role of properties such as hydrogen bonding.

For the present data only $\tilde{\nu}_f^{\circ}$, s, and a are used. The absence of easily hydrogen-bond forming available hydrogen atoms in DCTMPPD allows for setting b to 0. Inclusion of b as adjustable parameter (i) did not improve the result (R value) and (ii) yielded a value for b smaller than it's corresponding standard deviation. In Table 2, the fitted parameters plus their standard deviations and t-Student values [35] are represented.

These results show that the fluorescence of DCTMPPD is affected by two solute–solvent interactions: (i) First and most important are the polarity/polarizability effects, which are represented by a high value for s, with very small standard deviation and high t-value. (ii) Second and less important is α, which is manifested by a much smaller parameter value and a noticeable smaller t-Student value. This fact indicates certain hydrogen bonding acceptance ability of DCTMPPD. The multiple linear regression equation (LSER) for the fluorescence centers of gravity (in 10^3 cm^{-1}) using π^*- and α-values is shown in Fig. 9 and is described by the following equation:

$$\tilde{\nu}_f^{cg} = 20.09 - 1.60\pi^* - 0.34\alpha. \quad (12)$$

The negative signs for both, s and a coefficients can be explained by shifts of the fluorescence spectra to lower energies due to both interactions.

Before analyzing the experimental data by applying more fundamental methods we will resume the empirical results of the preceding analysis: (i) The E_T30 analysis only indicates that DCTMPPD is differently affected by the solvents than the Reichardt standard molecule. Anyway, two parallel plots, one for protic and one for aprotic solvents, are obtained where the protic solvents are displaced to higher wavenumbers than expected, indicating that DCTMPPD is less affected by hydrogen

Table 2
LSER parameters for the analysis of the fluorescence centres of gravity

Data	$\tilde{\nu}_f^{\circ}$	s	a	R
All data (25)	20.08 ± 0.05(433.4)	−1.48 ± 0.08(−18.9)	−0.39 ± 0.07(−5.9)	0.9782
Wo halogenated (23)	20.09 ± 0.03(572.4)	−1.55 ± 0.06(−25.2)	−0.36 ± 0.05(−7.2)	0.9887
Wo hal. + arom. (20)	20.09 ± 0.03(607.4)	−1.60 ± 0.06(−26.6)	−0.34 ± 0.05(−7.0)	0.9916

The parameters are given together with their respective standard deviations and the t-Student test values.

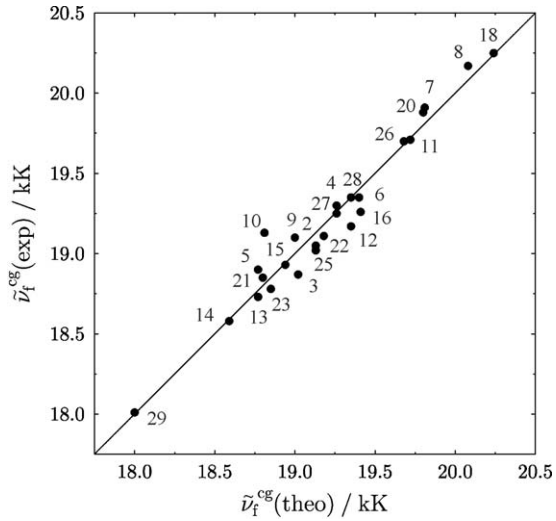

Fig. 9. LSER plot of experimental fluorescence maxima (all data except 1, 17, 19, 24) against their corresponding theoretical values using the α and π^* values for the solvent only.

bonding interactions than the Reichardt molecule. (ii) The LSER analysis already gives deeper insight into both qualitative and quantitative contributions to the solute–solvent interactions. Its result indicates that polarity/polarizability and to a small extent hydrogen bonding are the important interactions in condensed media. From a qualitative point of view these obtained results seem quite reasonable:

a. Polarity/polarizability term: the two electron donating (amino) and accepting (cyano) groups, respectively, are intrinsically adscribing the molecule a certain dipole moment which will definitely be strongly affected by various different solvent dipoles.
b. Solute basicity (hydrogen bond acceptor): qualitatively the two amino N atoms, and to some minor extent the cyano N atoms, possess a pair of free electrons that can interact with hydrogen atoms from protic solvents.
c. Solute acidity (hydrogen bond donor): the only hydrogen atoms available in DCTMPPD are the amino methyl hydrogens and the two aromatic hydrogen atoms, neither of which are known as strong hydrogen bond donors, hence b is of no importance.

The LSER analysis thus shows to be in good agreement with what is expected from a qualitative point of view.

3.5.3. Non-specific solute–solvent interactions

By changing the electronic properties of the solvents, represented by their continuum properties, dielectric constant, ε, and refractive index, n, a noticeable change in shape and position of the electronic transitions can be observed depending on the solute's electronic properties, as dipole moment, μ_x, and polarizability, α_x, of a given electronic state X. The relative value of the two latter quantities determines whether a solvatochromic shift will be more or less pronounced in absorption or fluorescence spectra. Unless α_x and μ_x are 0, a change in the corresponding electronic transition can be observed and should, for coherence reasons, be included in any solvatochromic shift analysis. From this point of view four different solute–solvent interactions can arise [36]: (i) dipole–dipole, (ii) solute dipole–solvent polarizability, (iii) solute polarizability–solvent dipole and (iv) polarizability–polarizability interactions. Four different models, all based on the Onsager reaction field [37] were used. They differ in their modelization of the solute molecule and the amount of interactions included in the reaction field:

a. **Lippert-Mataga model** [38]: the most simple model that accounts only for dipole–dipole interactions. The molecule is modelled by a sphere with radius r and assumes parallel ground and excited state dipole moments.

$$\tilde{\nu}_f^{cg} = \tilde{\nu}_{f0}^{cg} - \frac{2\mu_e(\mu_e - \mu_g)}{hcr^3}\left(\underbrace{\frac{\varepsilon - 1}{2\varepsilon + 1}}_{f(\varepsilon)} - \underbrace{\frac{n^2 - 1}{2n^2 + 1}}_{f(n^2)}\right), \quad (13)$$

where $\tilde{\nu}_{f0}^{cg}$ denotes the fluorescence transition in the absence of solvent, μ_e and μ_g denote the excited and ground state dipole moments, respectively, while the other parameters have their usual meaning.

b. **Spherical Lippert model** [39]: it accounts for dipole–dipole and solute dipole–solvent polarizability interactions using a spherical approximation of the solute molecule and parallel dipole moments:

$$\begin{aligned}\tilde{\nu}_f^{cg} &= \tilde{\nu}_{f0}^{cg} - \frac{2\mu_e(\mu_e - \mu_g)}{hcr^3}(f(\varepsilon) - f(n^2)) \\ &\quad - \underbrace{\frac{2(\mu_e^2 - \mu_g^2)}{2hcr^3} f(n^2)}_{\text{solvent polarizability}} \\ &= C - \frac{2\mu_e(\mu_e - \mu_g)}{hcr^3} f(\varepsilon) + \frac{(\mu_e - \mu_g)^2}{hcr^3} f(n^2) \quad (14)\end{aligned}$$

c. **Elliptic Lippert model** [39]: as b but using a more realistic elliptic approximation of the molecule (described by the three elliptical semiaxes a_e, b_e, c_e and an empirical factor r that can be approximated by the reduced solute radius as given in a):

$$\begin{aligned}\tilde{\nu}_f^{cg} &= \tilde{\nu}_{f0}^{cg} - \frac{2\mu_e(\mu_e - \mu_g)}{hcr^3} \underbrace{F(\varepsilon, A)}_{\text{ellipsoid}} f(\varepsilon) \\ &\quad + \frac{(\mu_e - \mu_g)^2}{hcr^3} \underbrace{F(n^2, A)}_{\text{ellipsoid}} f(n^2), \quad (15)\end{aligned}$$

where

$$F(x, A) = \frac{3A(1 - A)(2\varepsilon + 1)}{2((1 - A)\varepsilon + A)}$$

$$A = \frac{a_e b_e c_e}{2} \int_0^\infty \frac{ds}{(s + a_e^2)^{3/2}(s + b_e^2)^{1/2}(s + c_e^2)^{1/2}}$$

d. **Liptay model** [40]: the Liptay model represents the most comprehensive approach used in this paper and accounts for

all four possible solute–solvent interactions assuming ellipsoidal solute molecules. It's simplifications consist in assuming parallel dipole moments in the ground and excited state and setting ground and excited state solute polarizability equal:

$$\tilde{\nu}_{\mathrm{f}}^{\mathrm{cg}} = \tilde{\nu}_{\mathrm{f0}}^{\mathrm{cg}} - \frac{2\mu_{\mathrm{e}}(\mu_{\mathrm{e}}-\mu_{\mathrm{g}})}{hcr^3} F(\varepsilon, A)\underbrace{(1-f\bar{\alpha})}_{\text{solute pol.}} f(\varepsilon) + \frac{(\mu_{\mathrm{e}}-\mu_{\mathrm{g}})^2 - 2hcD}{hcr^3} F(n^2, A)\underbrace{(1-f'\bar{\alpha})}_{\text{solute pol.}} f(n^2), \quad (16)$$

where $F(x, A)$ and A are given by the above equations (in c), $\bar{\alpha}$ is the molecule's polarizability in the dipole moment direction,[4] D denotes the dispersion interactions[5] and f and f' are given by $f = 2r^{-3}f(\varepsilon)F(\varepsilon, A)$ and $f' = 2r^{-3}f(n^2)F(n^2, A)$, respectively.

Model a has the advantage of using a simple linear fit ($\tilde{\nu}_{\mathrm{f}}^{\mathrm{cg}}$ versus $f(\varepsilon) - f(n^2)$) to extract the excited state dipole moment, μ_{e}. The other three models require non-linear fitting procedures. In the case of large dipole moment changes upon excitation all models can be reduced to linear expressions in $f(\varepsilon) - 1/2f(n^2)$.

Not all solvent data was taken into account for the analysis. One has to restrict the solvents to those that don't show any specific solute–solvent interactions: (i) Hydrogen donating solvents ($\alpha > 0$ from Kamlet–Taft scale) were excluded to avoid interference with specific interactions. (ii) Dioxane was excluded due to it's general abnormal behaviour in solvent plot representations probably based either on conformation polarization from the non-polar chair- to the dipolar boat-form or solute–dipole–solvent quadrupole interactions [41]. (iii) Aromatics were excluded for their strong deviation from linearity to exceptionally lower wavenumbers, implying a certain stabilization mechanism between them and DCTMPPD.

With the remaining data the excited state solute dipole moment, μ_{e} can be estimated. The necessary ground state dipole moment, μ_{g}, was calculated to be 5.3 D, using the RHF method with a 6-31G* basis set. Experimental estimations of the ground state dipole moment, applying the Debye equation [42] gave a value of the same order of magnitude as the theoretically obtained one, however a more detailed study was prohibited due to the limited solubility of the investigated compound. For the determination of the excited state dipole moment the calculated value for μ_{g} was used. The solute radius, r, was evaluated to be 5.1 Å from an elliptical subscription to the geometry optimized structure minimizing the ellipsoid's superficies. The solvent plot analysis results obtained using the four different models are resumed in Table 3. For a representative plot of the data using the Liptay model confer to Fig. 10. It can be concluded that the solute dipole–solvent dipole interaction (Lippert-Mataga model) is the main factor in determining DCTMPPDs excited state solvatochromism. Neither the introduction of the solvent polarizability (Lippert models) nor the additional inclusion of the solute polarizability (Liptay model) improve the results.

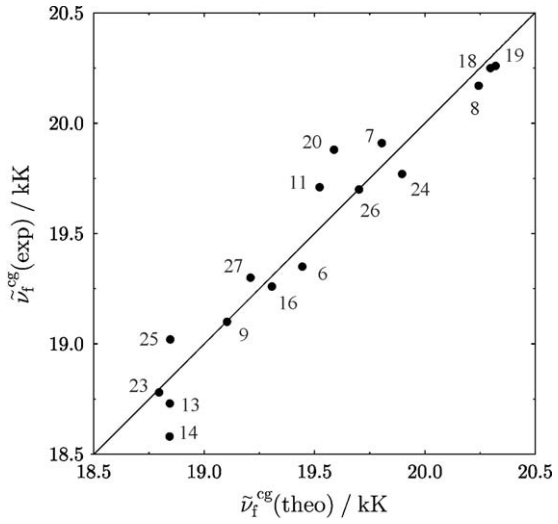

Fig. 10. Experimental fluorescence centers of gravity against their corresponding theoretical values using the Liptay equation (16).

Table 3
Parameters obtained from non-specific solute–solvent interaction models

Model	$\tilde{\nu}_{\mathrm{f0}}^{\mathrm{cg}}$ (kK)	μ_{e} (D)	R
Lippert-Mataga	20.3	11.1	0.948
Lippert spherical	21.0	11.1	0.966
Lippert elliptic	21.1	12.5	0.962
Liptay	20.9	11.4	0.967

3.6. Acid–base properties in the aqueous phase

3.6.1. Ground state pK_{a}

The buffer solution absorption spectra of DCTMPPD in the pH range from 1.5 to 6.5 are shown in Fig. 11. Isosbestic points were found at 409, 342, 303 and 280 nm.

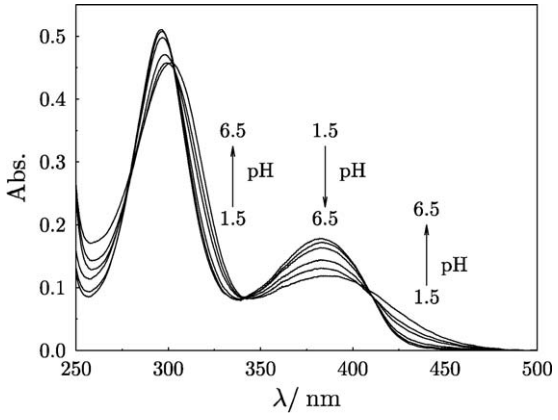

Fig. 11. Absorption spectra of DCTMPPD in NaH_2PO_4/citric acid-buffer solutions in the range of 1.5 <pH< 6.5 showing clearly the four isosbestic points at 279, 303, 342 and 409 nm, respectively.

[4] $\bar{\alpha}$ was calculated according to $\bar{\alpha} = \boldsymbol{\alpha}\vec{\mu}/|\vec{\mu}|$, where $\boldsymbol{\alpha}$ is the polarizability tensor and $\vec{\mu}$ is the ground state dipole moment vector from RHF calculations.

[5] $D \sim 0$ for benzene-like molecules [36].

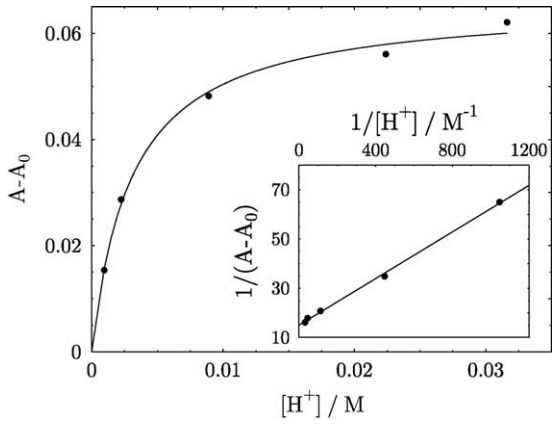

Fig. 12. Representation of absorption titration data at 382 nm according to Eq. (17). The inlet shows the double-reciprocal linear Benesi-Hildebrandt type representation.

Analysis of the simple reaction scheme:

$$\mathrm{DCTMPPD} + \mathrm{H_3O^+} \underset{k_{dp}}{\overset{k_p}{\rightleftharpoons}} \mathrm{DCTMPPDH^+} + \mathrm{H_2O}$$

enables one to obtain the familiar equation [43,44]:

$$A - A_0 \sim (\epsilon_{\mathrm{DH^+}} - \epsilon_{\mathrm{D}}) \frac{K_c[\mathrm{H^+}]}{1 + K_c[\mathrm{H^+}]} \tag{17}$$

where $K_c = [\mathrm{HD^+}]/([\mathrm{H^+}][\mathrm{D}]) = 1/K_a$ and A and A_0 are the absorptions at a given proton concentration, $[\mathrm{H^+}]$, and of the totally unprotonated form, respectively. The pK_a values were extracted performing either (i) a double reciprocal Benesi-Hildebrand analysis (inlet Fig. 12) or (ii) a hyperbolic fitting of the above equation to the experimental data at various wavelengths. The latter, preferably used [44], method is represented for one wavelength in Fig. 12. For both analysis methods the same ground state acidity constant of the protonated form, $pK_a = 2.5$, was found.

3.6.2. Excited state pK_a^*

The excited state protonation equilibrium constant was determined by two different methods, namely (i) by applying the Förster cycle [45,46] and (ii) from steady-state fluorescence titrations [47].

3.6.2.1. Förster cycle. The determination of pK_a^* using the Förster cycle is obtained by applying [40,48],

$$pK_a^* = pK_a - \frac{\tilde{\nu}_{00} - \tilde{\nu}'_{00}}{RT \ln 10} - \frac{\Delta S_{solv}}{R \ln 10} \tag{18}$$

where $\tilde{\nu}_{00}$ and $\tilde{\nu}'_{00}$ denote the 0–0 transition energies obtained from the average of the absorption and fluorescence centers of gravity of protonated and unprotonated form, respectively. ΔS_{solv} is the change in entropy of solvation due to the change of the solute's dipole moment on excitation:

$$\Delta S_{solv} = \frac{3}{r^3(2\varepsilon + 1)^2(1 - 2\alpha f(\varepsilon)/r^3)^2} \frac{\mathrm{d}\epsilon}{\mathrm{d}T}(\mu_e^2 - \mu_g^2), \tag{19}$$

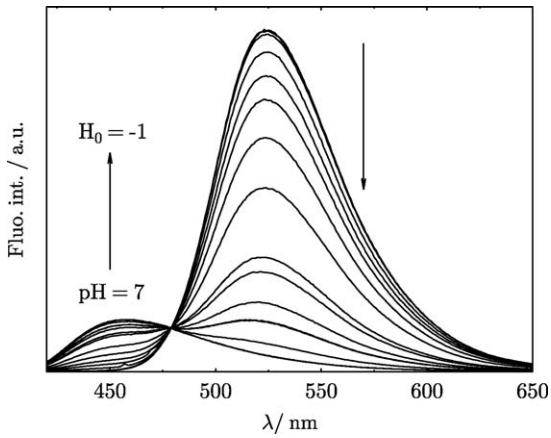

Fig. 13. Fluorescence spectra of DCTMPPD at different pH (H_0).

where ε is the dielectric constant, r the mean solute radius and $f(\varepsilon)$ is defined as in Eq. (13). The obtained pK_a^* value amounts to 0.3 ± 0.5.

3.6.2.2. Steady-state fluorescence titration. Less problems are encountered when performing steady-state fluorescence titrations in the case of molecules where both forms, protonated and unprotonated, fluoresce. The fluorescence spectra, obtained by excitation in the energetically lowest lying isosbestic point (at 409 nm), were corrected for different absorption (including the bandpass of the apparatus) and refractive indices of the corresponding samples

$$\Phi_{corr} = \frac{\Phi_{exp} n^2}{1 - 10^{-A}}. \tag{20}$$

Decomposition of the fluorescence spectra into protonated and deprotonated forms, via multilinear regression, yields the relative quantum yields, Φ/Φ_0 and Φ'/Φ'_0, of unprotonated and protonated forms, respectively. The corrected experimental data are depicted in Fig. 13 showing an isoemissive point at 478 nm.

The relative intensities are then represented against the corresponding acidity function (pH or H_0) yielding two sigmoid-like curves whose points of inflection, situated at pH 1.8 is a measure for the dissociation constant in the excited state, pK_a^* (Fig. 14).

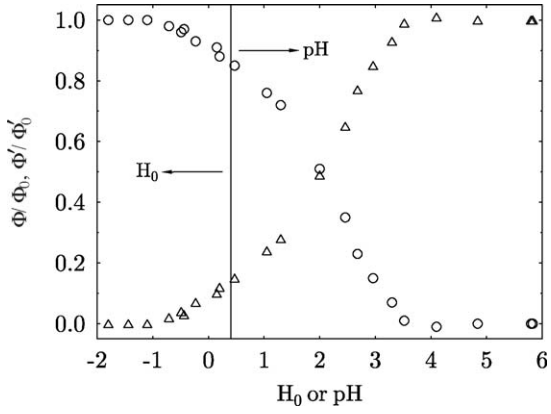

Fig. 14. Relative fluorescence intensities of protonated (◯) and deprotonated forms (△), respectively, against the corresponding pH and H_0 values.

For an easier extraction of pK_a^* the $\log(\Phi/\Phi')$ is plotted against the pH/H_0 scale (not shown) and the intersection with the abscissa yields pK_a^* [49].

The unsymmetric behaviour of the titration curve might be due to (i) the change from the pH to the H_0 scale, whose values were obtained from literature [50], (ii) due to the fact that the ionic strength was not held constant over the entire titration range, or (iii) due to the fact that the excited state equilibrium is not fully established during the lifetime of both excited state species. Especially the protonation reaction of the excited base seems to be too slow to completely evolve during the short lifetime of the protonated form (4 ns). The observed excitation wavelength dependence of the relative fluorescence contributions of protonated and unprotonated species indicates the non-triviality of the excited state proton transfer "equilibrium", the clarification of which will be the topic of further investigations.

4. Concluding remarks

DCTMPPD has been shown to display a high fluorescence quantum yield (ranging from 0.37 to 0.58) in a great variety of solvents, with the fluorescence lifetime ranging from 12.2 to 22.9 ns increasing with solvent polarity. The lowest singlet excited state has a dipole moment of about 6 D larger than the ground state one, therefore showing quite remarkable solvatochromism. Anyhow, the anisotropy measurements, the mirror symmetry between absorption and emission and the coincidence between experimental radiative lifetimes and those calculated using the Strickler-Berg approximation, suggest that the geometry of the emitting state is quite similar to that of the ground state and that the absorption and emission transition dipole moments are almost parallel. The sensitivity to the solvent acidity (α) is quite low ($a \sim s/3$). In water solutions both excited and ground state pK_a are close to 2, though due to slow rates in the excited state it is difficult to quantitatively define the pK_a^*. The intersystem crossing quantum yield to the excited triplet subsystem is so small that even in frozen solutions the phosphorescence signal is extremely low.

As compared to other related compounds the first appreciable difference is the high fluorescence quantum yield: no other *p*-phenylenediamine reaches values higher than 0.2 [51]. It is clear that electron donating groups combined with the withdrawing cyano moieties favour a lower excited singlet state of appropriate symmetry with a high radiative decay rate constant. From another point of view, DCTMPPD does not show any detectable dual fluorescence. In that way it behaves as 3,5-dicyano-aminobenzene (35DCAB), what is quite reasonable [53]. As DCTMPPD, 35DCAB displays a long fluorescence lifetime [53], but to the best of the authors' knowledge no quantum yield has been published. Another molecule to compare with is the *m*-cyano-*N*,*N*-dimethylaniline (3DMABN), but the published data of this molecule are somehow contradictory, since Ref. [52] gives a lifetime of 23.2 ns in acetonitrile at 25 °C while Ref. [54] gives 10.7 ns and a quantum yield of 0.28 in similar conditions. The authors did not find any data concerning 2,6-dicyano-aniline, or its *N*-methyl substituted cousin, a molecule which would have been quite interesting to be compared with DCTMPPD. Mono cyano substituted *p*-phenylenediamines are also absent from the photochemistry literature.

The comparison with 35DCAB and 3DMABN [53,54] may help in the understanding of the photophysical characteristics of DCTMPPD. It is generally accepted that the ^1L_a and ^1L_b orbitals of the mono-substituted benzenes become mixed when a group like CN is placed in the meta position with respect to the amino moiety. This induces an increase in the polarity of the excited state and a related noticeable sensitivity to solvent polarity as is the case for DCTMPPD. Furthermore, this stabilization precludes the system from undergoing an adiabatical charge separation. Additionally, this would explain how the non-radiative rate constant decreases when solvent polarity increases: both, quantum yield and fluorescence lifetime, increase in going from cyclohexane to acetonitrile, following the 0–0 energy gap. In fact, the effect seems to saturate in solvents of medium polarity (cf. Table 1) although this observation is possibly masked by some other specific interactions. Though there are competitive theories trying to explain the properties of the cited molecules, it seems clear that the lower excited state is stabilized with respect to the higher one. Again, this would explain how the yields and lifetimes increase with polarity as both states separate further.

To conclude, we have here presented many data on a highly fluorescent *p*-phenylenediamine showing its sensitivity to the solvent properties. The results are coherent with previous findings from other groups [53,54]. Further experiments on the photochemistry of this and other cyano-substituted *p*-phenylenediamines will be soon published.

Acknowledgements

The authors would like to thank A. Kapturkiewicz from the Institute of Physical Chemistry, Polish Academy of Sciences in Warszawa for the possibility to measure low-temperature emission spectra, and A. Kelterer for providing theoretical values for polarizability and ground state dipole moment. Furthermore the authors appreciate very much the instructive discussions with P. Jacques, Mulhouse, France. A.R. is deeply indebted to D.R. Kattnig for valuable help and discussions concerning Matlab based programming. Financial support of the EC's ERASMUS exchange programme, the Federal Ministry for education, science and culture and the Austrian Exchange Service are gratefully acknowledged.

References

[1] L. Michaelis, E.S. Hill, J. Am. Chem. Soc. 55 (1933) 1481.
[2] L. Michaelis, S. Granick, M.P. Schubert, J. Am. Chem. Soc. 61 (1939) 1981.
[3] G. Grampp, P. Pluschke, Collect. Czech. Chem. Commun. 52 (1987) 819.
[4] L. Michaelis, S. Granick, J. Am. Chem. Soc. 65 (1943) 1747.
[5] U. Nickel, E. Haase, W. Jaenicke, Ber. Bunsenges. Phys. Chem. 81 (1977) 849.
[6] G. Grampp, G. Stiegler, Z. Phys. Chem. NF 141 (1984) 185.
[7] M. Sacher, G. Grampp, Ber. Bunsenges. Phys. Chem. 101 (1997) 971.
[8] H. Honma, H. Murai, K. Kuwata, Chem. Phys. Lett. 195 (1992) 239.
[9] H. Murai, H. Honma, K. Kuwata, Z. Phys. Chem. 182 (1993) 31.

[10] H. Murai, A. Matsuyama, Y. Iwasaki, K. Enjo, K. Maeda, T. Azumi, Appl. Magn. Reson. 12 (1997) 411.
[11] Z.R. Grabowski, K. Rotkiewicz, W. Rettig, Chem. Rev. 103 (2003) 3899.
[12] G. Schwarzenbacher, B. Evers, I. Schneider, A. de Raadt, J. Besenhard, R. Saf, J. Mater. Chem. 12 (2002) 534.
[13] J. Jasny, J. Lum. 17 (2) (1978) 149.
[14] M. Berger, J.A. Bell, C. Steel, J. Chem. Edu. 52 (3) (1975) 191.
[15] S. Landgraf, Spectrochim. Acta A 57 (2001) 2029.
[16] J.R. Lakowicz, Principles of Fluorescence Spectroscopy, 2nd ed., Kluwer Academic/Plenum Publishers, New York/London/Moscow, 1999.
[17] G.A. Reynolds, K.H. Drexhage, Opt. Commun. 13 (1975) 222.
[18] J.B. Birks, Photophysics of Aromatic Molecules, 1st ed., Wiley Monographs in Chemical Physics, Wiley-Interscience, London, 1970.
[19] M. Balón, G. Angulo, C. Carmona, M.A. Muñoz, P. Guardado, M. Galán, Chem. Phys. 276 (2002) 155.
[20] S.I. Kotelevskiy, J. Lum. 79 (1998) 211.
[21] G. Angulo, G. Grampp, S. Landgraf, A. Rosspeintner, Unpublished Results.
[22] http://webbook.nist.gov.
[23] H. Laguitton-Pasquier, R. Pansu, J.-P. Chauvet, P. Pernot, A. Collet, J. Faure, Langmuir 13 (1997) 1907.
[24] A.S.E. Koti, M.M.G. Krishna, N. Periasamy, J. Phys. Chem. A 105 (2001) 1767.
[25] D.B. Siano, D.E. Metzler, J. Chem. Phys. 51 (3) (1969) 1856.
[26] A.S.E. Koti, N. Periasamy, Proc. Indian Acad. Sci. (Chem. Sci.) 113 (2001) 157.
[27] P. Wahl, Biophys. Chem. 10 (1979) 91.
[28] B. Valeur, Molecular Fluorescence, 1st Edition, Wiley-VCH, Weinheim, 2001.
[29] R.L. Christensen, R.C. Drake, D. Phillips, J. Phys. Chem. 90 (1986) 5960.
[30] G. Angulo, G. Grampp, A. Rosspeintner, Spectrochim. Acta A 65 (2006) 727.
[31] Y. Marcus, The Properties of Solvents, Wiley Series in Solution Chemistry, John Wiley & Sons Ltd, 1998.
[32] S.J. Strickler, R.A. Berg, J. Chem. Phys. 37 (4) (1962) 814.
[33] C. Reichardt, Solvents and Solvent Effects in Organic Chemistry, 2nd revised ed., Verlag VCH, Weinheim, 1990.
[34] M.J. Kamlet, R.W. Taft, Acta Chem. Scand. B 39 (1985) 611.
[35] I.N. Bronstein, K.A. Semendjajew, Taschenbuch der Mathematik, 25th ed., B. G. Teubner Verlagsgesellschaft, Stuttgart, 1991.
[36] P. Suppan, N. Ghoneim, Solvatochromism, 1st ed., The Royal Society of Chemistry, Cambridge, 1997.
[37] L. Onsager, J. Am. Chem. Soc. 58 (1936) 1486.
[38] E. Lippert, Z. Naturforschg. 10a (1955) 541.
[39] E. Lippert, Z. Elektroch. 61 (8) (1957) 962.
[40] W. Liptay, Z. Naturforschg. 20a (1965) 1441.
[41] P. Suppan, J. Photochem. Photobiol. A 50 (1990) 293.
[42] A. Bonilla, B. Vassos, J. Chem. Edu. 54 (1977) 130.
[43] H.A. Benesi, J.H. Hildebrand, J. Am. Chem. Soc. 71 (1949) 2703.
[44] R.B. Martin, J. Chem. Edu. 74 (10) (1997) 1238.
[45] T. Förster, Z. Elektroch. 54 (1) (1950) 42.
[46] A. Weller, Prog. Reac. Kin. 1 (1961) 187.
[47] H.H. Richtol, B.R. Fitch, Anal. Chem. 46 (12) (1974) 1749.
[48] K. Rotkiewicz, Z.R. Grabowski, Trans. Faraday Soc. 65 (1969) 3263.
[49] N. Chattopadhyay, J. Photochem. Photobiol. A 88 (1995) 1.
[50] M.A. Paul, F.A. Long, Chem. Rev. 57 (1) (1957) 1.
[51] I.B. Berlman, Handbook of Fluorescence Spectra of Aromatic Molecules, 2nd ed., Academic Press, New York, 1971.
[52] K.A. Zachariasse, T. von der Haar, A. Hebecker, U. Leinhos, W. Kühnle, Pure Appl. Chem. 65 (8) (1993) 1745.
[53] K.A. Zachariasse, Chem. Phys. Lett. 320 (2000) 8.
[54] W. Rettig, B. Bliss, K. Dirnberger, Chem. Phys. Lett. 305 (1999) 8.